

# Exploring charge density distribution and electronic properties of hybrid organic-germanium layers

Flávio Bento de Oliveira

*Universidade Federal de Goiás, Institute of Physics,  
Campus Samambaia, 74690-900 Goiânia, Goiás, Brazil*

Erika Nascimento Lima

*Universidade Federal de Rondonópolis,  
ICEN, Rondonópolis, Mato Grosso, Brazil*

Andreia Luisa da Rosa

*Universidade Federal de Goiás, Institute of Physics,  
Campus Samambaia, 74690-900 Goiânia, Goiás, Brazil and  
Bremen Center for Computational Materials Science,  
University of Bremen, Am Fallturm 1, 28359 Bremen, Germany*

Mauricio Chagas da Silva

*Bremen Center for Computational Materials Science,  
University of Bremen, Am Fallturm 1, 28359 Bremen, Germany  
Max Planck Institute for the Structure and Dynamics of Matter; Luruper Chaussee 149,  
Geb. 99 (CFEL), 22761 Hamburg, Germany and  
Université de Lorraine, CNRS, LPCT, F-54000 Nancy, France*

Thomas Frauenheim

*Bremen Center for Computational Materials Science,  
University of Bremen, Am Fallturm 1, 28359 Bremen, Germany and  
Computational Science Research Center, No.10 East Xibeiwang Road,  
Beijing 100193 and Computational Science and Applied Research Institute Shenzhen, China.*

## Abstract

Band gap tuning and dielectric properties of small organic ligands adsorbed on bidimensional germanium monolayers (germanene) have been investigated using first-principles calculations. We show that the adsorption of these small groups retains the initially stable free-standing pristine buckled germanium nanostructures. Charge density and chemical bonding analysis show that the ligands are chemisorbed on the germanium layers. Finally we demonstrate that the dielectric properties of bare and ligand adsorbed germanene have a large anisotropy. Our findings of a finite gap shows open a path for rational design of nanostructures with possible applications in biosensors and solar cells.

## I. INTRODUCTION

The study of two-dimensional materials has increasing interest after the discovery of graphene whose property differed surprisingly from its three-dimensional form, graphite<sup>1,2</sup>. These materials have electronic properties of great interest for technological applications. Graphene in its honeycomb structure has a zero gap, with conduction and valence bands being degenerate at K and K points, forming cones. However, difficulties in carrying out and adjusting a reasonable sizeable band gap in graphene is attracting increasing interest in other two-dimensional materials.

Recent investigations suggest that germanene react rapidly with the environment<sup>3</sup>. This may affect not only their electronic structure, but also their reactivity, dielectric and optical properties. Therefore one may search for ways of tuning the electronic properties of these two-dimensional structures. A promising route was demonstrated using adsorption of organic molecules or functional groups<sup>4</sup>. It has been shown that modified germanene were stable hybrid materials and with tunable optical properties<sup>3</sup>. Although bare germanium layers have been extensively investigated, functionalized layers with organic molecules has received less attention. Theoretical investigations by Kou and co-authors proposed that adsorption of  $-\text{CH}_2\text{OCH}_3$  groups on germanene could lead to ferroelectric properties<sup>5</sup>. Furthermore it has been suggested that hydrogen adsorbed layers become topological insulators when external strain is applied<sup>6</sup>.

In this work we have investigated the electronic and dielectric properties of germanene with small organic groups using first-principles calculations. We show that the some of the adsorbed structures possess a sizeable band gap. We claim that the stability of these structure is a combined effect of both in-plane strain induced by the adsorption of organic groups and ligand-ligand interactions. Finally we show that the dielectric properties of this material have a large anisotropy.

## II. METHODOLOGY

We employ density functional theory<sup>7,8</sup> within the generalized gradient approximation<sup>9</sup> and the projected augmented wave method (PAW)<sup>10,11</sup> as implemented in the VASP code<sup>11</sup> to investigate the electronic structure germanene hybrid layers. A  $(1 \times 1)$  supercell containing

two germanium atoms was employed. Forces on atoms were converged until  $10^{-4}$  eV/Å. A vacuum region of 10 Å has been found to be sufficient to avoid spurious interactions between germanene layers in neighbouring cells. A  $(10 \times 10 \times 1)$   $\mathbf{k}$ -point sampling has been used in the calculations of all investigated systems with an energy cutoff of 500 eV. The calculation of the dielectric function was performed using the GW method<sup>12</sup>. A  $(8 \times 8 \times 1)$   $\mathbf{k}$ -points mesh has been employed. The electron localization function visualization was obtained using the VESTA software<sup>13</sup> and the critical point analysis was provided by the post-process of the total electronic density using Critic2 software<sup>14,15</sup>.

### III. RESULTS AND DISCUSSIONS

#### A. Structural properties

The structural stability of the buckled and planar structure has been investigated by varying the in-plane lattice parameter  $a$  and fully relaxing all the atoms in the unit cell. The relaxed bare buckled structure is shown in Fig. 2(a). The inclusion of spin-orbit coupling does not change the lattice parameter, but it lowers the total energies of the bare structure as shown in Fig.1. The optimized in-plane lattice parameter for buckled (planar) germanene is  $a = 4.05 \text{Å}$  ( $4.11 \text{Å}$ ). The buckled structure is 0.2 eV energetically more stable than the planar one. The Ge-Ge distance is 2.43 Å, as shown in Table I. This result is in good agreement with previous calculations<sup>5,16</sup>.

Table I: Lattice parameter  $a$ , Ge-Ge distance, Ge-ligand distance, buckling of germanium modified structures calculated within GGA.

	$a$	Ge-Ge	Ge-C	Ge-H	buckling
bare	4.05	2.43			0.69
-H	4.08	2.47		1.57	0.74
-COOH	4.20	2.52	2.08		0.74
-CH3	4.11	2.50	2.00		0.78
-CH <sub>2</sub> OCH <sub>3</sub>	4.24	2.55	2.02		0.71
-CH <sub>2</sub> CHCH <sub>2</sub>	4.40	2.65	2.05		0.73

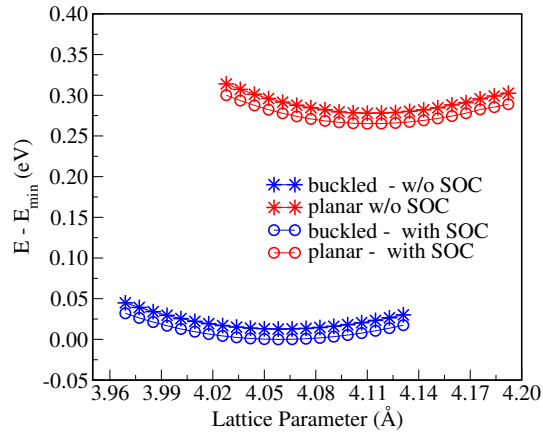


Figure 1: (color online) Total energy of buckled and planar germanium layers with and without spin-orbit coupling. The zero of energy is set to the lowest energy of the buckled structure calculated within GGA.

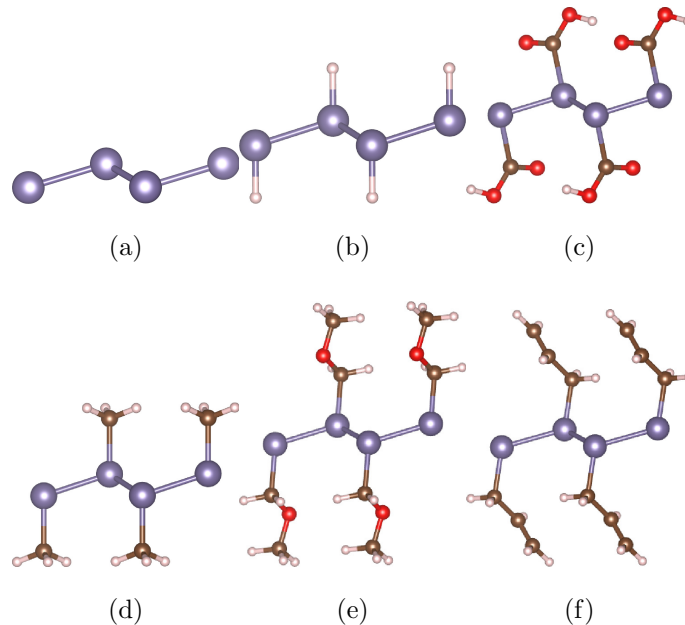


Figure 2: (color online) Side view of relaxed germanium layers adsorbed with organic ligands at 1 ML regime: a) buckled bare, b) hydrogen, c)  $\text{-COOH}$ , d)  $\text{-CH}_3$ , e)  $\text{CH}_2\text{OCH}_3$  and f)  $\text{CH}_2\text{CHCH}_2$ . Red, brown, blue, white and magenta are oxygen, carbon, hydrogen and germanium atoms, respectively.

We have investigated the following ligands: -H, -CH<sub>3</sub>, -COOH, -CH<sub>2</sub>CHCH<sub>2</sub> and -CH<sub>2</sub>OCH<sub>3</sub> groups, since these groups were synthesized experimentally<sup>3</sup>. The relaxed bare and functionalized germanene are shown in Fig. 2. We have considered structures with ligands adsorbing on top positions of germanium atoms on both sides of the germanium surface. Although we cannot rule out that smaller coverages may be present, we should point out that higher coverages yield to more stable structures in germanene<sup>3</sup>. Upon adsorption of ligands, the initially buckled geometry of germanene has a slight different buckling compared to the bare layers, as shown in Table I. This is rather different from what has been found for similar groups on bismuthene which become planar upon adsorption of ligands<sup>5,17,18</sup>. As a general feature, the intralayer lattice parameter  $a$  and consequently Ge-Ge distance increases as the ligand size increases. This means that the ligand-ligand interaction plays an important role on the stabilization of the hybrid structures.

The in-plane lattice parameter of H-Ge shown in Fig. 2 (b) is 4.08 Å with Ge-Ge bond length of 2.47(Å). The Ge-COOH structure is shown in Fig. 2 (c) and has  $a = 4.20$  Å and Ge-Ge distance of 2.52 Å. The Ge - CH<sub>3</sub> structure shown in Fig. 2 (d) has  $a = 4.11$  Å and Ge-Ge distance of 2.50. This is similar to other small groups due to similar van der Waals radii. The in-plane lattice constant is somewhat larger for Ge - CH<sub>2</sub>CHCH<sub>2</sub> shown in Fig. 2 (e) (4.21 Å) and Ge - CH<sub>2</sub>OCH<sub>3</sub> seen in Fig. 2 (f) (4.40 Å). In particular, the ligands in the later two structures assume a tilted configuration. One can conclude that the not only the ligand size but also its character is important to determine the bond strength.

#### IV. CHEMICAL BONDING ANALYSIS

The nature of the chemical bonds in the hybrid systems was investigated by calculating the charge density difference between the electronic densities of the adsorbed germanium layers and their constituent systems. The electronic density difference shown in Fig. 3 is given by  $\Delta\rho = \rho^{\text{Ge-X}} - \rho^{\text{Ge}} - \rho^{-\text{X}}$ , where  $\rho^{\text{Ge-X}}$  is the electronic density of the hybrid Ge-X layers,  $\rho^{\text{Ge}}$  and  $\rho^{-\text{X}}$  are the charge densities of the germanium layers and the ligand, respectively, calculated at fixed atomic positions after structure optimization. As a general feature, charge accumulation on the ligand (yellow) and charge withdrawal (blue) close to the germanium atom is seen.

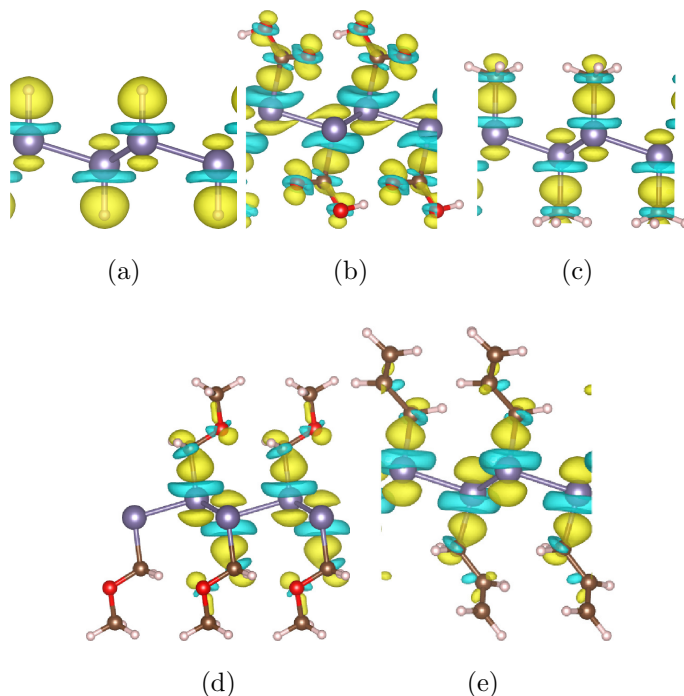


Figure 3: Charge density difference of modified germanene structures with a) -H, b) -COOH, c) -CH<sub>3</sub>, d) CH<sub>2</sub>OCH<sub>3</sub> and e) CH<sub>2</sub>CHCH<sub>2</sub>. Blue indicates a loss of electrons whereas yellow indicates accumulation of electrons. Isosurface levels are set to  $0.002 e/\text{\AA}^3$ .

Ge-H hybrid layers shown in Fig. 3(a) have a larger electron density at hydrogen atoms and a withdraw of electrons at germanium sites. Ge-COOH also shows accumulation of charge at the ligand, mainly on oxygen and carbon atoms, while charge is withdrawn at germanium sites as shown in Fig. 3(b). The complex Ge-CH<sub>3</sub> shown in shows that electronic charge is accumulated the ligand upon adsorption on the germanene. Furthermore, between C and Ge bonds there is an excess of electrons as it can be seen in Fig. 3(c) . The Ge-CH<sub>2</sub>OCH<sub>3</sub> hybrid also shows accumulation of charge at the ligand, mainly on the oxygen and carbon atoms, while charge is depleted at the germanium site, as shown in Fig. 3(d). The complex Ge-CH<sub>2</sub>CHCH<sub>2</sub> also shows accumulation of electrons on the ligand oxygen and carbon atoms, while regions close to the germanium are depleted of electrons. At the germanium site and also between C and Ge bonds there is an excess of electrons as seen in Fig. 3(e). One can therefore conclude that due to the charge accumulation/withdraw in the modified germanium layers, the reactivity of the whole system changes. This could be quite useful for further docking of organic or biomolecules.

In order to extend our understanding on the chemical environment of Ge-X layers, the electron localization function (ELF) and topological features of the bonding critical points (BCP) were evaluated. The ELF helps us to understand how electrons are distributed around the atoms. ELF value close to 1 correspond to regions where there is a high probability of finding electronic density characterizing non-bonded electrons or covalent bonds. On the other hand, ELF values close to 0.5 indicates regions where electrons are delocalized like in metallic bonds. As a general feature, Fig. 4 shows a cross section of the ELF for bare and Ge-X layers. In all systems, there is a localized electronic density region between germanium atoms. This region between germanium bonds is located at half distance between germanium atoms, indicating a covalent bond type.

For buckled germanene, shown in Fig. 4(a), a localized region right above and below the germanium atoms is seen. This region is associated to the non-bonded electrons present in this system. This comes from the fact that germanium is four-fold coordinated and in buckled germanium one chemical bond is missing, thus leaving out one non-bonded electron per germanium atom.

For the functionalized systems, shown in Figs. 4 (b)-(f), it is also seen an localized electronic density region between germanium and hydrogen/carbon bonds. Differently from the Ge-Ge bonds, Ge-H and Ge-C bonds are slightly asymmetric. Therefore, we can conclude that chemical bonds between Ge-H and Ge-C are polarized, specially for the larger organic groups. Despite the polarization seen between Ge-X bonds, the shared electron regions are also present between the Ge-C distances, which is also an indication of covalent-like bonds.



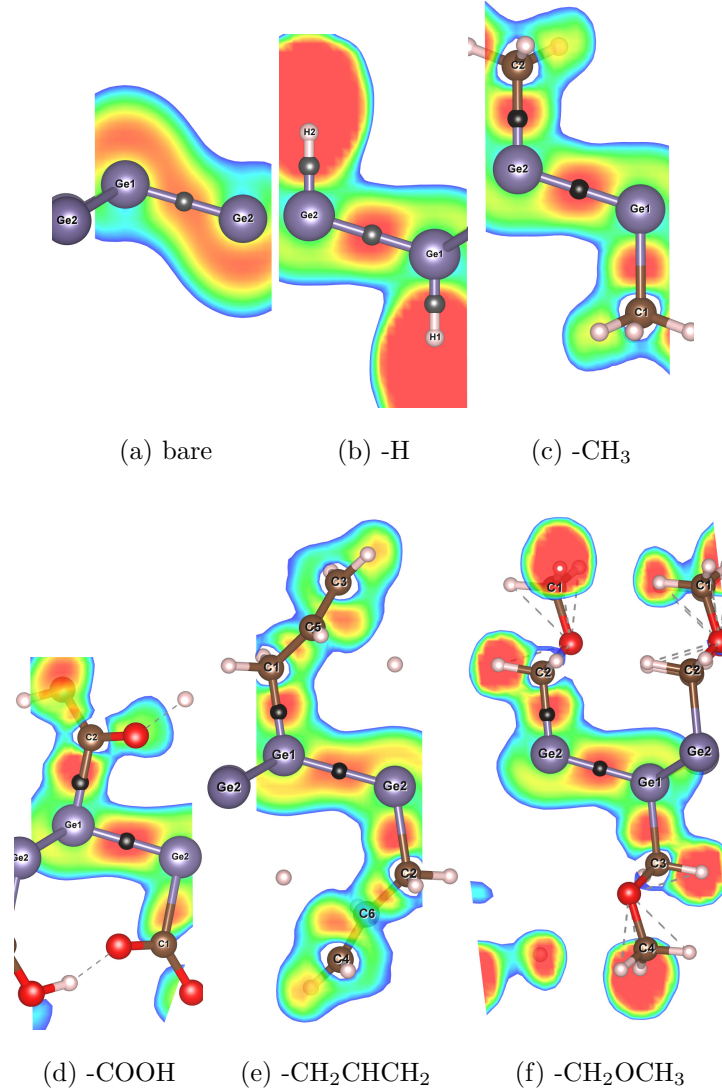


Figure 4: Cross section of the electron localization function (ELF) and the main critical points between Ge-Ge and Ge-X bonds (black spheres) for the modified germanene layers.

ELF values are expressed between 0.5 (blue surfaces) and 0.9 (red surfaces) .

In Fig.(4) we see the main bonding critical points (BCP) between Ge-Ge and Ge-X atoms. The BCP are in agreement with the ELF, which indicates shared electrons regions between the Ge-Ge, Ge-H and Ge-X atoms. The interpretation of the CP give us the nature of the chemical environment along the bonds. For light atoms in the chemical bonds, large values of the electronic density at the BCP ( $\rho_{BCP}$ ) and a negative value of its Laplacian ( $\nabla^2\rho_{BCP}$ ) are indication of shared electrons interactions<sup>19,20</sup>. However, we do not have light atoms

only. Thus, the Laplacian can assume any positive or negative value close to zero for shared electrons regions (covalent-like bonds)<sup>21,22</sup>. The values for  $\rho_{BCP}$  and  $\nabla^2\rho_{BCP}$  are presented in Table (II) and (III). For Ge-X bonds the  $\rho_{BCP}$  presents values close to  $0.1 \text{ e}\text{\AA}^{-3}$  whereas for Ge-Ge bonds the value is smaller and close to  $0.06\text{-}0.07 \text{ e}\text{\AA}^{-3}$ . For non-interacting regions with weak interactions, such as van der Waals complexes for example  $\rho_{BCP}$  is usually much smaller than the values seen for Ge-Ge or Ge-X bonds. The Laplacian values for Ge-Ge bonds are all negative and close to zero, as it can be seen in Table (III), whereas  $\nabla^2\rho_{BCP}$  of the Ge-X bond are close to zero and the signals in general are positive, Table (II) .

Table II: The topological features of the Ge-X bonding critical point on the different chemical environment of buckled and Ge-ligand layers.

Property	-H	-CH <sub>3</sub>	-COOH	-CH <sub>2</sub> OCH <sub>3</sub>	-CH <sub>2</sub> CHCH <sub>2</sub>
$\rho_{BCP}$	0.127	0.116	0.105	0.117	0.109
$\nabla^2\rho_{BCP}$	-0.066	0.053	0.013	0.057	-0.007
$G(\rho_{BCP})$	0.092	0.079	0.067	0.081	0.072
$V(\rho_{BCP})$	-0.200	-0.145	-0.131	-0.147	-0.145
$H(\rho_{BCP})$	-0.108	-0.066	-0.064	-0.067	-0.073
$V(\rho_{BCP})/G(\rho_{BCP})$	2.179	1.832	1.952	1.824	2.023
$H(\rho_{BCP})/\rho_{BCP}$	-0.854	-0.569	-0.608	-0.567	-0.671

Table III: The topological features of the Ge-Ge bonding critical point on the different chemical environment of buckled and Ge-ligand layers.

Property	Bare	-H	-CH <sub>3</sub>	-COOH	-CH <sub>2</sub> OCH <sub>3</sub>	-CH <sub>2</sub> CHCH <sub>2</sub>
$\rho_{BCP}$	0.073	0.073	0.071	0.070	0.065	0.058
$\nabla^2\rho_{BCP}$	-0.014	-0.023	-0.027	-0.030	-0.032	-0.024
$G(\rho_{BCP})$	0.037	0.037	0.035	0.034	0.030	0.025
$V(\rho_{BCP})$	-0.077	-0.080	-0.076	-0.075	-0.068	-0.056
$H(\rho_{BCP})$	-0.040	-0.043	-0.042	-0.041	-0.038	-0.031
$V(\rho_{BCP})/G(\rho_{BCP})$	2.092	2.153	2.194	2.222	2.266	2.241
$H(\rho_{BCP})/\rho_{BCP}$	-0.549	-0.581	-0.587	-0.594	-0.587	-0.535

The evaluation of  $\rho_{BCP}$  and  $\nabla^2\rho_{BCP}$  is not sufficient to characterize the nature of the chemical bond of more complex system like Ge-X layers. Energetic features as kinetic energy density  $G(\rho_{BCP})$ , the potential energy density  $V(\rho_{BCP})$  and the total energy density  $H(\rho_{BCP})$  can also be helpful for interpreting the nature of the chemical bond. Bianchi *et al.*<sup>23</sup> suggested that  $G(\rho_{BCP}) \ll |V(\rho_{BCP})|$ ,  $V(\rho_{BCP}) \ll 0$  and  $H(\rho_{BCP}) \ll 0$  are indicative of the presence of the covalent bonds. For the BCP between Ge-X,  $G(\rho_{BCP})$  is much smaller than the  $|V(\rho_{BCP})|$ , as seen in Tab II. However, for Ge-Ge bonds,  $G(\rho_{BCP})$  is smaller and closer to  $|V(\rho_{BCP})|$ , Tab III. The evaluated values for  $V(\rho_{BCP})$  and  $H(\rho_{BCP})$  are negative for both BCP at Ge-Ge and Ge-X bonds, Tab II and Tab III. These energetic conditions indicate shared electrons interactions, i.e., covalent bonds between Ge-Ge and Ge-X.

The ratios  $|V(\rho_{BCP})|/G(\rho_{BCP})$  and  $H(\rho_{BCP})/\rho_{BCP}$  are other topological quantities which are used to address the nature of the chemical bond environment<sup>21,22,24</sup>. For covalent bonds, it is common to obtain the ratio  $|V(\rho_{BCP})|/G(\rho_{BCP}) > 2$ , in intermediate bond cases such as high polarized and ionic interactions it is found  $1 < |V(\rho_{BCP})|/G(\rho_{BCP}) < 2$ . Table III shows  $|V(\rho_{BCP})|/G(\rho_{BCP}) > 2$  for all Ge-X layers critical points between Ge-Ge indicating the presence of a covalent bonds. For the critical points localized between Ge-X atoms, the values are smaller and/or closer to 2. This indicates polarized covalent bonds between Ge-C atoms, as it can be seen in Table II. The other ratio  $H(\rho_{BCP})/\rho_{BCP}$  feature is smaller than zero for all localized critical points which is also an indicative of covalence between the

### A. Electronic properties

In order to understand the interaction between ligand and the substrate, we have calculated the individual orbital contributions to the band structure, as shown in Fig. 5. The  $p_{xy}$ ,  $p_z$  and  $s$  contributions are shown. Bare germanium layers have a metallic character and zero gap with a linear dispersion at the  $\Gamma$  point, as it is seen in Fig.5 (a). Band-to-band  $\Gamma - \Gamma$  and  $\Gamma$ -M energy transitions are reported in Table IV.

As the size of ligand increases, the band gap decreases. It is smaller upon adsorption of -H and larger upon adsorption of  $-\text{CH}_2\text{OCH}_3$ . The band structure for Ge-H is shown in Fig. 5(b), for Ge -  $\text{CH}_3$ (c) in Fig. 5(c), for Ge-COOH in Fig. 5(d) and for Ge -  $\text{CH}_2\text{OCH}_3$  in Fig. 5(e).

Contributions to the states close to the Dirac point are mainly due to  $p_{xy} = p_x + p_y$  and  $p_z$  orbitals. Upon ligand adsorption on germanium layers, the Dirac cone moves from K to  $\Gamma$  point. All these hybrid structure have now a sizeable band gap. The exception is the Ge -  $\text{CH}_2\text{CHCH}_2$ , which shows metallic character, as shown in Fig. 5(f). This can be understood considering that this group is an electron donor and therefore renders a metallic system.

$-\text{CH}_2\text{OCH}_3$  induces electron capture and induces band gap opening. This can be explained by noting the  $-\text{CH}_2\text{OCH}_3$  group is an electron acceptor. This means that the ligand character is also important to determine the bond strength and consequently the electronic structure of the hybrid system.

We can clearly see contributions from the functional groups at VBM and CBM, implying that we have formation of bonds between the ligand and the germanium layers. The change in the band gap is in agreement with suggestions of Ref. <sup>3</sup>. Our values are somewhat underestimated compared to experimental ones.

The dielectric function of hybrid germanene-organics layers were investigated by calculating the imaginary part of the dielectric function at GW level. The imaginary part of the dielectric function is calculated directly from the electronic structure through the joint density of states and the momentum matrix elements occupied and unoccupied eigenstates according Ref.<sup>12</sup>.

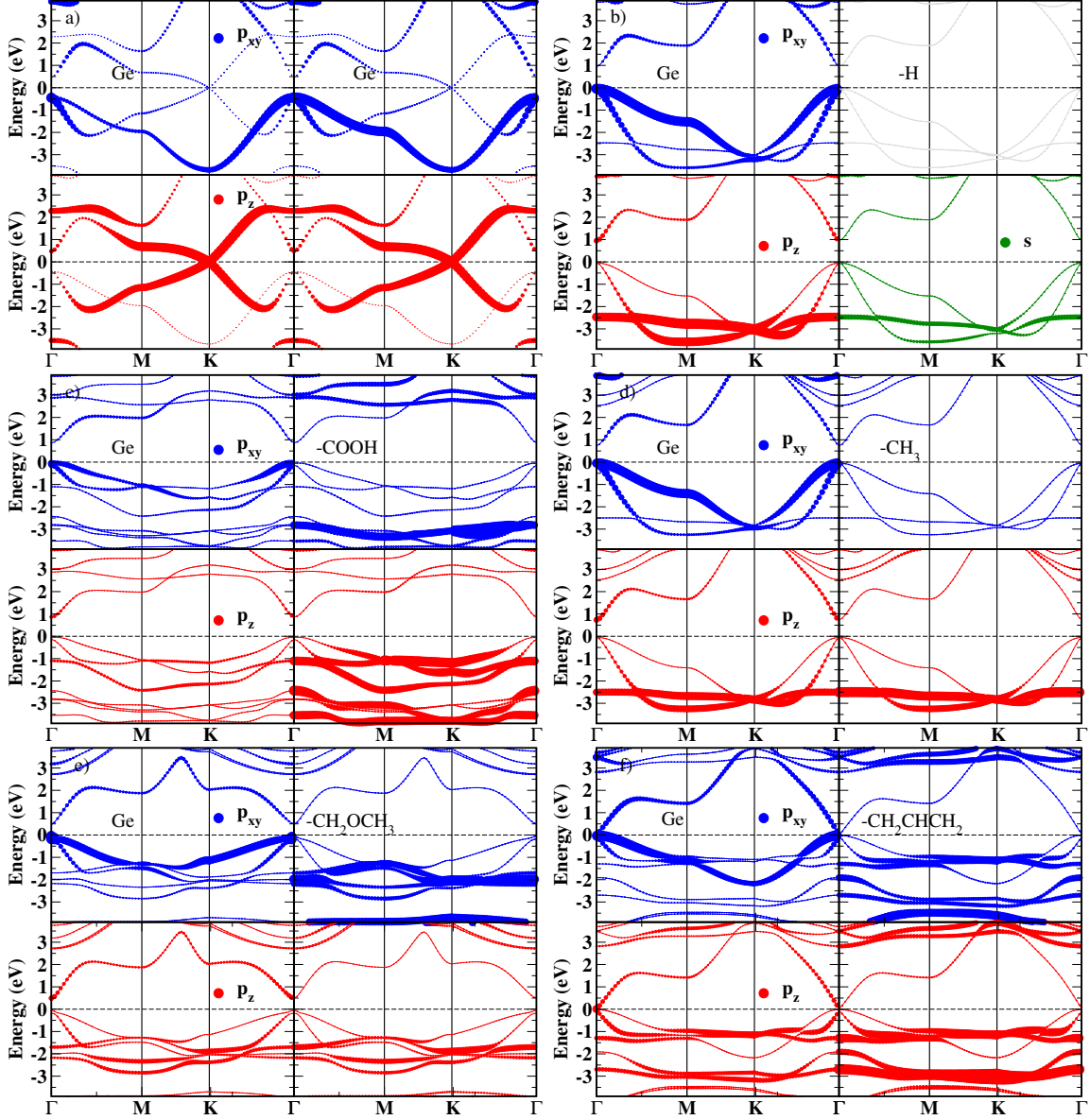


Figure 5: Orbital resolved band structure of modified germanene structures. a) germanene, b) germanane, c)  $-\text{COOH}$ , d)  $-\text{CH}_3$ , e)  $-\text{CH}_2\text{OCH}_3$  and f)  $\text{CH}_2\text{CHCH}_2$ . The zero of energy is set to the VBM.

We show the dielectric function calculated within the  $G_0W_0$  and GW approximations in Fig. 6. The averaged parallel  $\varepsilon_{\parallel} = (\varepsilon_{xx} + \varepsilon_{yy})/2$  and perpendicular  $\varepsilon_{\perp} = \varepsilon_{zz}$  components of the the imaginary part of the dielectric function  $\varepsilon_2$  are shown. The  $\varepsilon_{\parallel}$  component corresponds to the propagation of the external electromagnetic field parallel to the germanene plane while  $\varepsilon_{\perp}$  corresponds to the field perpendicular to the plane. Because of optical selection rules, anisotropy in the optical spectra is seen. Anisotropy has also been reported in layered

monochalcogenide of germanium sulfide (GeS)<sup>25</sup>, black phosphorous<sup>26</sup> and bismuthene<sup>16</sup>.

The systems with a gap show finite absorption limits for both parallel and perpendicular directions with larger intensity for the ( $\epsilon_{\parallel}$  component).

Table IV: Energy gaps and transitions (in eV) corresponding to Fig. 6) of ligand modified germanene calculated within GGA,  $G_0W_0$  and GW.

ligand	gap			1 <sup>st</sup> peak		2 <sup>nd</sup> peak		Exp. <sup>3</sup>
	PBE	$G_0W_0$	GW	$G_0W_0$	GW	$G_0W_0$	GW	
bare (metal)								
-H	0.99	2.1	2.5	2.5	2.6	4.1	4.2	1.57
-COOH	0.91	2.0	2.4	0.9	2.5	2.1	4.0	
-CH <sub>3</sub>	0.78	1.7	2.1	0.8	2.0	2.4	3.6	1.66
-CH <sub>2</sub> OCH <sub>3</sub>	0.54	1.6	1.6	0.6	1.4	2.6	3.3	1.45
-CH <sub>2</sub> CHCH <sub>2</sub> (metal)								

As discussed in Ref.<sup>3</sup>, both ligand size and electronegativity can change the bond length and band gap of functionalized germanene. Larger ligands are expected to lead to larger Ge-Ge separation, thus yielding a lower band gap. Ligands with greater electronegativity are expected to withdraw electrons and therefore lower the band gap. The size of the ligands we have calculated decreases in the order  $-\text{CH}_2\text{CHCH}_2 < -\text{CH}_2\text{OCH}_3 < -\text{CH}_3 < -\text{H}$ . On the other hand ligand electronegativity decreases in the order from  $-\text{CH}_2\text{OCH}_3 < -\text{H} < -\text{CH}_3 < -\text{CH}_2\text{CHCH}_2$ . According to these experiments, the band gap should be inversely proportional to Ge-Ge bond length. The observed band gap value increases with decreasing ligand electronegativity, with the exception of Ge- $\text{CH}_2\text{CHCH}_2$ . The general conclusion is that ligands that are more electron-withdrawing and have greater steric bulk will expand the Ge-Ge framework and lower the band gap, with complete ligand coverage.

We find that the inclusion of self-consistency in the Green's functions leads to a blue shift compared to the  $G_0W_0$  results. The bare germanene shown in Fig. 6(a) has metallic behavior.  $G_0W_0$  increases the gap and  $\text{GW}_0$  increases further. As a general feature, two main absorption peaks appear in the spectrum. Ge-H shown in Fig. 6(b) has a peak at 2.5 eV

at  $G_0W_0$  and 2.6 eV at  $GW_0$ . A second peak appears at 4.1 and 4.2 eV, at  $G_0W_0$  and  $GW_0$  levels, respectively. The Ge-COOH spectrum shown in Fig. 6(c) has peaks at 0.9 and 2.5 eV. A second peak appears at 2.1 and 4.0 at  $G_0W_0$  and  $GW_0$  levels, respectively. A first peak at 0.8 and 2.0 for Ge-CH<sub>3</sub> are seen in Fig. 6(d) at  $G_0W_0$  and  $GW_0$  levels, respectively. Another peak at 2.4 and 3.6 eV appears at  $G_0W_0$  and  $GW_0$  levels, respectively. Last, Ge – CH<sub>2</sub>OCH<sub>3</sub> shows high intensity at at 0.6 and 1.4 eV, at  $G_0W_0$  and  $GW_0$  levels, as it can be seen in Fig. 6(e). On the other hand another peak appears at 2.6 and 3.3 eV  $G_0W_0$  and  $GW_0$  levels, Finally, we find that –CH<sub>2</sub>CHCH<sub>2</sub> is an electron donor and therefore renders the Ge–CH<sub>2</sub>CHCH<sub>2</sub> metallic.

According to Ref. <sup>3</sup> the absorption onset measured via Diffuse reflectance absorption (DRA) for germanium modified layers is 1.57 eV for Ge-H, 1.66 eV for GeCH<sub>3</sub>, 1.55 eV for GeCH<sub>2</sub>CHCH<sub>2</sub> and 1.45 eV for Ge-CH<sub>2</sub>OCH<sub>3</sub>. Our  $GW_0$  calculations are in reasonable agreement with these experimental results, since the band gap decreases with the ligand size. The exception is for Ge-CH<sub>2</sub>CHCH<sub>2</sub>, where the experimental value for the band gap is 1.55 eV, but we found this materials to be a metal. The reason for such discrepancy could be inferred taken into account the number of layers, coverage and adsorption site. However, further investigation is needed to clarify this aspect.

## V. CONCLUSIONS

We have performed first-principles calculations of germanene functionalized layers with small organic ligands. Our charge density analysis show that the ligands are chemisorbed on the germanium layers. Our calculations for the dielectric properties of bare and ligand adsorbed germanene show a large anisotropy and that the absorption onset is determined by both ligand electronegativity and size, in reasonable agreement with recent experimental results<sup>3</sup>. We believe our findings of a finite gap shows open a path for rational design of nanostructures with possible applications in biosensors and solar cells.

## VI. ACKNOWLEDGEMENTS

We acknowledge the financial support from the Brazilian Agency CNPq and German Science Foundation (DFG) under the program FOR1616. The calculations have been per-

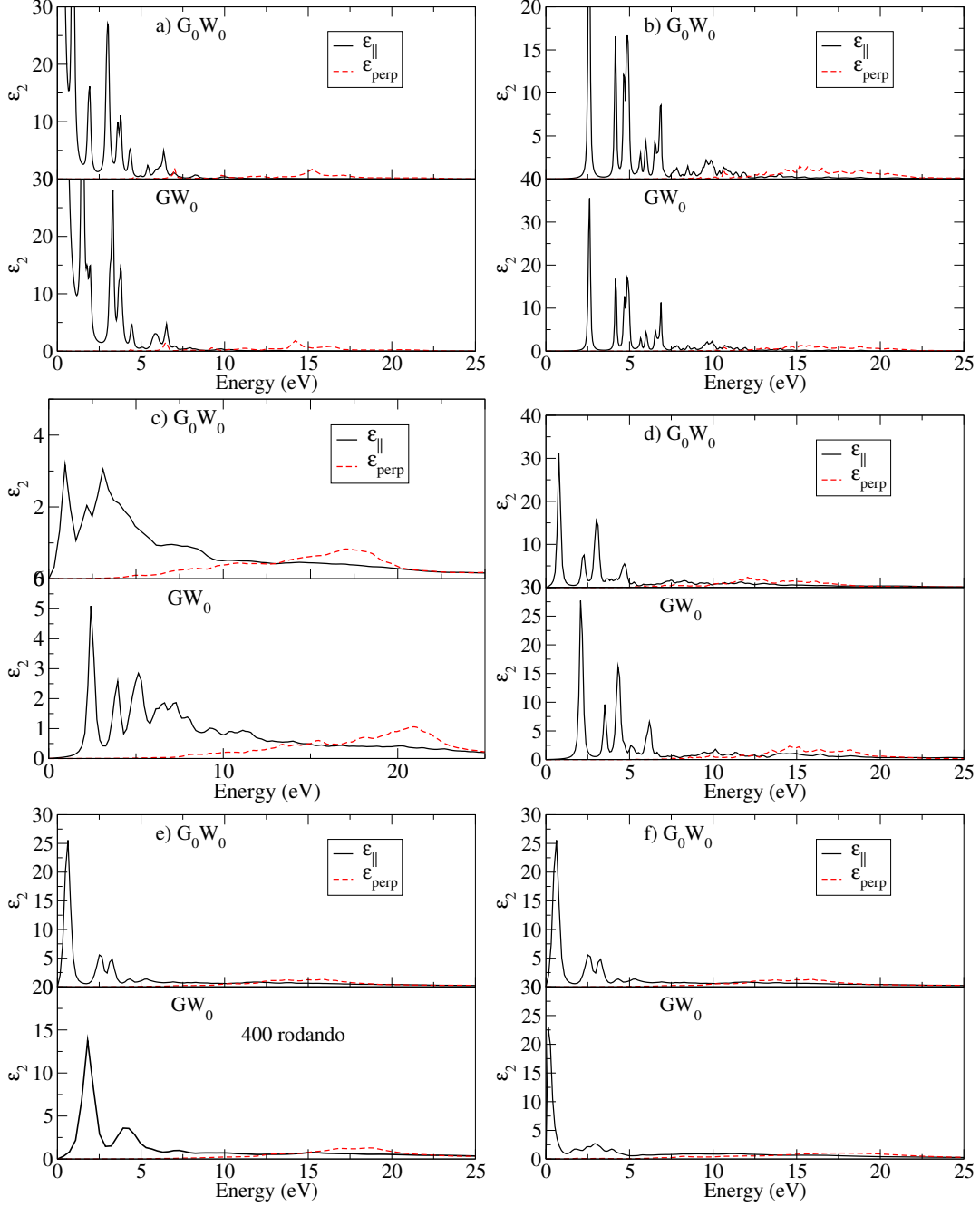


Figure 6: Imaginary part of the dielectric function for pure and functionalized germanene within  $G_0W_0$  (upper panel on each figure) and  $GW_0$  (lower panel on each figure) approximations. a) germanene, b) germanane, c)  $-\text{COOH}$ , d)  $-\text{CH}_3$ , e)  $-\text{CH}_2\text{OCH}_3$  and f)  $\text{CH}_2\text{CHCH}_2$ . Light propagation parallel to the germanium layer is denoted as  $\epsilon_{\parallel} = (\epsilon_{xx} + \epsilon_{yy})/2$ . Light propagation perpendicular to the germanium layers is denoted as

$$\epsilon_{\text{perp}} = \epsilon_{zz}.$$



formed using the computational facilities of Supercomputer Santos Dumont and at QM3 cluster at the Bremen Center for Computational Materials Science and CENAPAD.

---

- <sup>1</sup> K. Novoselov, A. Geim, S. Morozov, D. Jiang, Y. Zhang, S. Dubonos, I. Grigorieva, and A. Firsov, *Science* **306**, 666 (2004).
- <sup>2</sup> A. K. Geim and K. S. Novoselov, *Nature Materials* **6**, 183 (2007).
- <sup>3</sup> S. Jiang, S. Butler, E. Bianco, O. D. Restrepo, W. Windl, and J. E. Goldberger, *Nature Communications* **5**, 3389 (2014).
- <sup>4</sup> Y. Ren and Z. Q. and Qian Niu, *Reports on Progress in Physics* **79**, 066501 (2016).
- <sup>5</sup> L. Kou, H. Fu, Y. Ma, B. Yan, T. Liao, A. Du, and C. Chen, *Phys. Rev. B* (2018).
- <sup>6</sup> R. R. Q. Freitas, R. Rivelino, F. de Brito Mota, C. M. C. de Castilho, A. Kakanakova-Georgieva, and G. K. Gueorguiev, *JPCCC* **119**, 23599 (2015).
- <sup>7</sup> P. Hohenberg and W. Kohn, *Phys. Rev.* **136**, B864 (1964), URL <http://link.aps.org/doi/10.1103/PhysRev.136.B864>.
- <sup>8</sup> W. Kohn and L. J. Sham, *Phys. Rev.* **140**, A1133 (1965), URL <http://link.aps.org/doi/10.1103/PhysRev.140.A1133>.
- <sup>9</sup> J. P. Perdew, K. Burke, and M. Ernzerhof, *Phys. Rev. Lett.* **77**, 3865 (1996), URL <http://link.aps.org/doi/10.1103/PhysRevLett.77.3865>.
- <sup>10</sup> P. E. Blöchl, *Phys. Rev. B* **50**, 17953 (1994), URL <http://link.aps.org/doi/10.1103/PhysRevB.50.17953>.
- <sup>11</sup> G. Kresse and D. Joubert, *Phys. Rev. B* **59**, 1758 (1999), URL <http://link.aps.org/doi/10.1103/PhysRevB.59.1758>.
- <sup>12</sup> M. Shishkin, M. Marsman, and G. Kresse, *Phys. Rev. Lett.* **99**, 246403 (2007), URL <http://link.aps.org/doi/10.1103/PhysRevLett.99.246403>.
- <sup>13</sup> K. Momma and F. Izumi, *Journal of Applied Crystallography* **44**, 1272 (2011), ISSN 0021-8898, URL <http://scripts.iucr.org/cgi-bin/paper?S0021889811038970>.
- <sup>14</sup> A. Otero-de-la Roza, M. Blanco, A. M. Pendás, and V. Luaña, *Computer Physics Communications* **180**, 157 (2009), ISSN 00104655, URL <https://linkinghub.elsevier.com/retrieve/pii/S0010465508002865>.

- <sup>15</sup> A. Otero-de-la Roza, E. R. Johnson, and V. Luaña, *Computer Physics Communications* **185**, 1007 (2014), ISSN 00104655, URL <https://linkinghub.elsevier.com/retrieve/pii/S0010465513003718>.
- <sup>16</sup> D. Kecik, V. O. Özçelik, E. Durgun, and S. Ciraci, *Phys. Chem. Chem. Phys.* **21**, 7907 (2019), URL 10.1039/C8CP07344A.
- <sup>17</sup> A. L. da Rosa, E. N. Lima, M. C. da Silva, R. B. Pontes, J. S. de Almeida, T. M. Schmidt, and T. Frauenheim, *J. Phys. Chem. C* (2020), in print.
- <sup>18</sup> A. L. Rosa, E. N. Lima, R. B. Pontes, T. Schmidt, and T. Frauenheim (2020), submitted.
- <sup>19</sup> Bader and R. F. W., in *Atoms in Molecules: A Quantum Theory* (Oxford Univ. Press, Oxford, 1990), chap. 7. *Chemica*, pp. 248–351, ISBN 9780198558651.
- <sup>20</sup> S. Jenkins, *Journal of Physics: Condensed Matter* **14**, 10251 (2002), ISSN 0953-8984, URL <https://iopscience.iop.org/article/10.1088/0953-8984/14/43/321>.
- <sup>21</sup> P. Macchi and A. Sironi, *Coordination Chemistry Reviews* **238-239**, 383 (2003), ISSN 00108545.
- <sup>22</sup> P. Macchi, D. M. Proserpio, and A. Sironi, *Journal of the American Chemical Society* **120**, 13429 (1998), ISSN 0002-7863, URL <https://pubs.acs.org/doi/10.1021/ja982903m>.
- <sup>23</sup> R. Bianchi, G. Gervasio, and D. Marabello, *Inorganic Chemistry* **39**, 2360 (2000), ISSN 00201669.
- <sup>24</sup> E. Espinosa, I. Alkorta, J. Elguero, and E. Molins, *The Journal of Chemical Physics* **117**, 5529 (2002), ISSN 0021-9606, URL <http://aip.scitation.org/doi/10.1063/1.1501133>.
- <sup>25</sup> N. Research, *Nano Research* pp. 546–555 (2017).
- <sup>26</sup> A. N. Rudenko, S. Yuan, and M. I. Katsnelson, *Phy. Rev. B* **92**, 085419 (2015).